Hindawi
Geofluids
Volume 2021, Article ID 7153015, 11 pages
https://doi.org/10.1155/2021/7153015

Research Article

The Effects of Precrack Angle on the Strength and Failure Characteristics of Sandstone under Uniaxial Compression

Shuai Zhang,[1] **Jinhai Xu**,[1] **Liang Chen**,[1] **Hideki Shimada**,[2] **Mingwei Zhang**,[3] **and Haiyang He**[1]

[1]*State Key Laboratory of Coal Resources and Safe Mining, China University of Mining and Technology, Xuzhou 221116, China*
[2]*Department of Earth Resources Engineering, Faculty of Engineering, Kyushu University, 744 Motooka, Nishi-ku, Fukuoka 819-0395, Japan*
[3]*State Key Laboratory for Geomechanics and Deep Underground Engineering, China University of Mining and Technology, Xuzhou 221116, China*

Correspondence should be addressed to Jinhai Xu; ts20020122p21@cumt.edu.cn

Received 6 September 2021; Revised 23 September 2021; Accepted 24 September 2021; Published 14 October 2021

Academic Editor: Zhijie Wen

Characterization of the mechanical properties of cracked rock masses is essential for ensuring the long-term stability of the engineering environment. This paper is aimed at studying the relationship between the strength characteristics of specimen and the angle of precrack, as well as the interaction of cracks under uniaxial compression. To this end, two sandstone specimens, distinguished with a single and three precracks, were built using the PFC software. For the former case, both the peak strength and elastic modulus increase to a peak value as the crack angle α gets closer to the forcing (loading) direction. For the latter case, the strength experiences a trend of increasing-maintaining trend as the crack angle α gets closer to the forcing direction, and the elastic moduli are barely affected. For the specimens containing a single precrack, their crack numbers increased approximately in a one-step or two-step stair pattern with increasing axial strain; whereas for the specimens containing three cracks, their crack numbers all showed a multistep growth trend. Furthermore, the failure mode of the specimen is closely related to the precrack angle. However, if the precrack distribution does not affect the original crack propagation path, it will hardly affect the mechanical properties of the specimen.

1. Introduction

Rock is widely distributed on the earth's surface. As a natural material, inevitably, there are defects such as cracks inside the rock which are induced by thermal stress, erosion, earthquakes, human engineering disturbances, etc. [1–3]. As an example, at Hornelen, western Norway, sandstone and conglomerate fill a fault-enclosed basin, about 70×30 km, which is the remains of a once larger basin. The basin sediments are about 100~200 m thick and are of continuous transversal cycles, consisting of beds about 2 m thick. The cracks and joints there caused by the long-time affection of low temperature and ocean erosion have been extremely developed [4–7], as shown in Figure 1. The existence of cracks not only reduces the material strength of the rock but also accelerates the damage process, which poses safety hazards to the construction of slopes and underground projects [2, 5, 7, 8]. Therefore, it is of great significance to study the strength characteristics of cracked specimens and the interaction of multiple cracks within the specimen.

The mechanical properties of defected rock mass have been a hot topic in the field of geotechnical engineering, and rich results have been achieved [2, 9–11]. Differing in the number of predefects, the current researches can be mainly grouped into two categories. The first type of research mainly focuses on rock mass, and the number of precracks reaches hundreds to thousands [5, 6, 12–14]; the second type of research focuses on laboratory specimen, and the number of predefects is generally less than four [15–17].

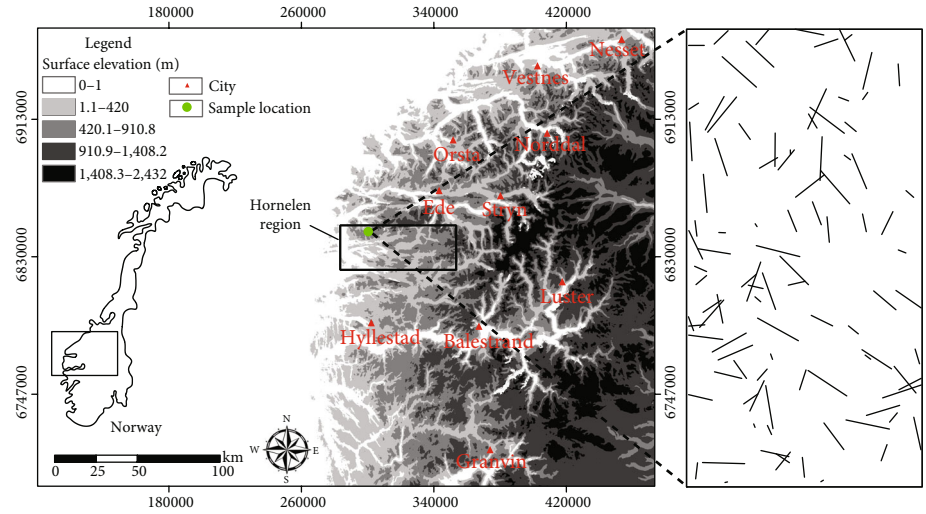

Figure 1: Outcrop map of the natural fracture system in the sandstone at Hornelen Basin, western Norway [5–7].

For the first type of research, due to the large size of the specimen, the current research mainly focuses on the location of rock damage [12], the fracture surface roughness [13, 18], and the specimen heterogeneity [5, 6]. Only a few studies have looked into the strength characteristics of specimens [2]. Shi et al. [2, 7] investigated the correspondence between crack distribution modes and rock mechanical properties, as well as the strength damage theory. However, the number of distributed cracks involved in the above studies is excessive; the crack propagation is thus affected by too many factors. As a result, it is hard to identify the influence of the crack interaction on the strength characteristics of the specimen.

For the second type of research, predefects are mainly made by hydraulic cutting (experiment) or the particle element deleting (numerical simulation). The elastic modulus, compressive strength, shear strength, and failure mode of the specimen were analyzed by changing its shape and size [16, 17], the confining pressure [19], or the angle [20–22] as well as the combination and number of predefects [10, 11]. These researches are of great significance for understanding the mechanical properties of defected rock, although large defects exist in crack prefabrication—the width of the cracks is larger than 2 mm [10, 14]. Therefore, the research object of this research in the strict sense is fissured rock mass rather than the commonly observed cracked rock mass in nature [5, 7]. The mechanical properties of cracked rock mass are obviously not equivalent to that of the fissured rock mass, and the research on cracked specimen is extremely insufficient. Moreover, the current researches on multifissured rock masses only focus on the combinations of fissures and lack a comparative analysis, so it is very hard to understand the specific impact of a fissure on the mechanical properties of a specimen [10, 23, 24].

In this paper, two sets of sandstone specimens differing in containing a single crack and three cracks were built using the PFC software. The relationship between the strength characteristics of the specimen and the angle of the precrack, as well as the interaction of cracks under uniaxial compression, was studied.

2. Numerical Model of Cracked Sandstone Specimen

2.1. Particle Flow Code (PFC). PFC^{2D} software is very convenient in realizing the crack prefabrication and is outstanding in simulating the mechanical properties and failure process of rock and soil medium [23]. Due to these advantages, the PFC^{2D} software was selected for the simulation in this study. The particles and the bonds between particles are used to characterize the medium in the software, where the particles are simulated with rigid body of unit thickness. Two types of bonding effects of rock media suitable for this simulation are selected, namely, contact bond and parallel bond, as shown in Figure 2. The contact bond reflects the normal and tangential interactions (forces) between particles (see Figure 2(a)), while the parallel bond transmits both the force and the moment (see Figure 2(b)). It is widely accepted that these two kinds of bonds both exist in the interior of rock and soil [7], so they are used in this paper.

2.2. Calibration of Sandstone Mesoscopic Parameters. To ensure the credibility of the simulation, it is necessary to determine the model parameters for the simulation. For PFC software, the particles and bonds are used to characterize the medium. Therefore, it is necessary to determine mesoscopic parameters that reflected the physical and mechanical properties of the particles and bonds. Due to the limitation in observation techniques, these parameters can hardly be obtained through laboratory tests. For uniaxial compression simulation with PFC, the "trial and error" method is usually used to calibrate the mesoscopic parameters of the specimen. As shown in Figure 3, m_i is the strength parameter of Hoek-Brown [27]. In this method, the full stress-strain curve and the corresponding failure mode of a representative specimen need to be firstly obtained through

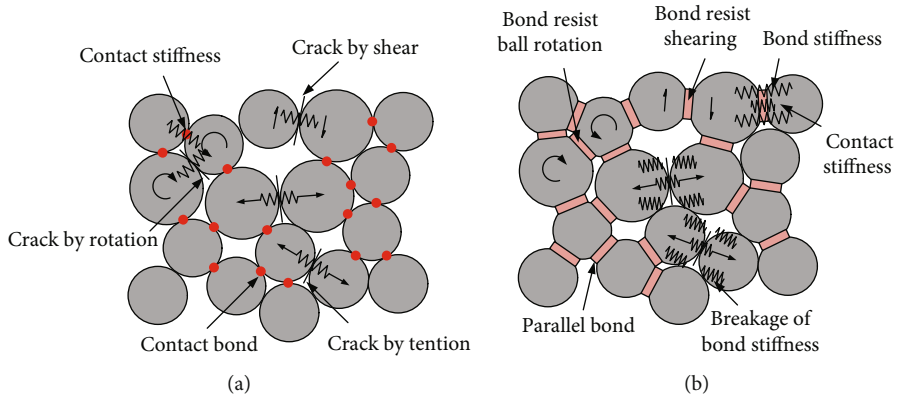

Figure 2: Cohesive model and its micromechanical behavior schematic diagram [7, 25, 26]: (a) contact bonds reflect the normal and tangential interactions (forces) between particles; (b) parallel bonds transmit both the force and the moment.

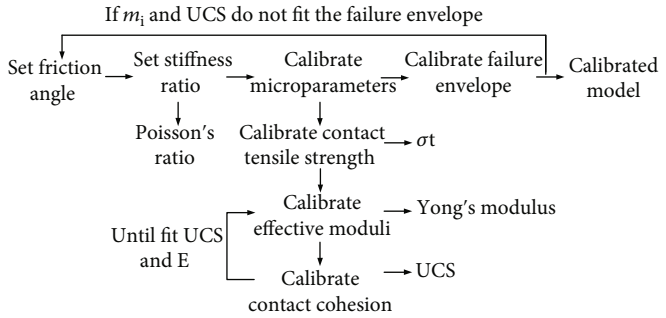

Figure 3: The "trial and error" method parameter checking process of the PFC model [27].

laboratory tests; next, a numerical model is established, and the parameters such as the stiffness, elastic modulus, and the tensile and cohesive strength are adjusted until the numerical curve is roughly consistent with the experimental curve; finally, fine-tune the parameters until the failure mode of the numerical specimen is consistent with that of the experimental specimen [27].

In this paper, the uniaxial compression tests on sandstone specimens were performed by the MTS815 test machine of the State Key Laboratory for Geomechanics and Deep Underground Engineering, China University of Mining and Technology, as shown in Figure 4. The size of the laboratory specimen is 50 mm by 100 mm (diameter and height), and the loading was controlled by displacement with the rate of 0.002 mm/timestep [2].

The intact sandstone model with 31190 particles was established using PFC^{2D} software. The size and loading strategy of the sandstone model are consistent with that of the laboratory test. The parameters of the numerical specimen were calibrated using the "trial and error" method. Model results are compared with the experimental data, showing the stress-strain curve and failure mode of the specimen in Figures 5 and 6, respectively.

As shown in Figures 5 and 6, the full stress-strain curve and the failure mode of the numerical specimen are qualitatively consistent with that of the experimental specimen. Note that the simulation curves deviate from the experimental ones in the prepeak stage, which is because that there is an obvious compaction stage for the laboratory specimen before the peak. To the best of our knowledge, this stage cannot be simulated by all numerical software including

Figure 4: MTS815 test machine.

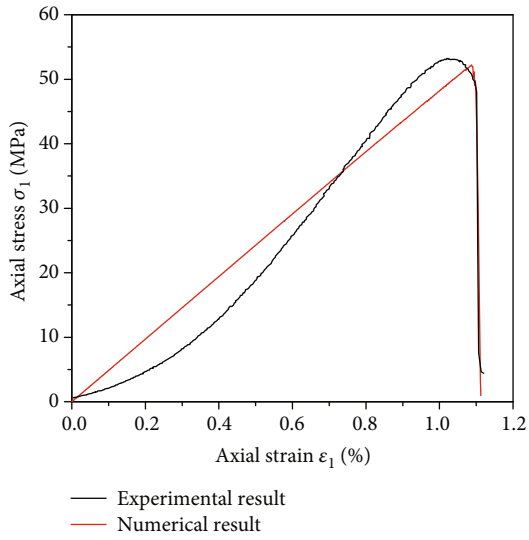

Figure 5: The comparison between the numerical and experimental stress-strain curves of intact sandstone specimens.

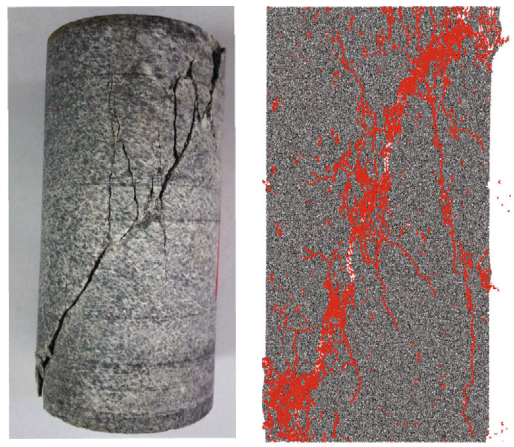

(a) (b)

Figure 6: Failure modes of intact sandstone specimens obtained through simulation and experiment: (a) experimental failure mode; (b) numerical failure mode.

PFC software [2, 14]. Currently, there are two main ways to cope with this problem. The first way is to ensure the consistency of the peak strength and peak strain with that of the actual specimen but might leave a difference in the elastic modulus [7, 28–30]. An alternative method is to ensure the elastic modulus and the peak strength to be consistent with that of the actual specimen but might lead to a significant difference in the peak strain [14].

Considering the study of rock strength to be the priory focus of this research, the first approach was chosen. Furthermore, the relative errors of peak strength and peak strain are 1.7% and 3.8%, respectively. The simulation results qualitatively agree with the experimental results, and the simulation parameters truly reflect the mechanical characteristics of the laboratory specimen.

Table 1: Mesoscopic parameters of the PFC^{2D} medium.

Parameters	Value
Minimum particle size (mm)	0.1
Maximum particle size (mm)	0.3
Density (kg/m^3)	2700
Porosity	0.15
Contact bond modulus (GPa)	0.6
Contact bond stiffness ratio	1.0
Friction coefficient	0.8
Parallel bond tensile strength (MPa)	26.5
Parallel bond cohesion (MPa)	32
Parallel bond friction angle (°)	32.5
Parallel bond modulus (GPa)	8.7
Parallel bond stiffness ratio	1.0

The microscopic parameters of the intact sandstone specimen determined by the "trial and error" method are listed in Table 1.

2.3. Numerical Model of Sandstone Specimen with a Single Crack or Three Precracks. In PFC^{2D}, crack, as a planar and finite-sized discrete element, is characterized by a segment with two vertex object ends. The prefabrication of the crack is realized through the Discrete Fracture Network (DFN). In the DFN module of PFC software, the input parameters to realize the prefabrication of each crack are the length, angle, and center point, with the width of the crack to be insignificant [23, 31–34]. In order to study the relationship between the strength characteristics and the angle of the precrack, as well as the interaction of the cracks, two sets of specimens that contain a single crack and three cracks were established, as shown in Figure 7.

It can be seen from Figure 7(a) that each specimen in the first group contains one precrack, and the angle of the crack is set as 0°, 30°, 60°, 90°, 120°, and 150°, respectively. The lower left corner of the specimen is set as the coordinate origin, and the x and y coordinates of the crack center point are 25 mm and 50 mm, respectively. In the second group, two extra fixed-angle precracks were added on the basis of the specimens in the first group, denoted as precracks ② and ③. For cracks ② and ③, their angles are both 45° and their center points are located at (25 mm, 75 mm) and (25 mm, 25 mm), respectively, as shown in Figure 6(b). In addition, the crack lengths of the precracks in Figure 7 are all 25 mm. The smooth joint model was used to describe the mechanical properties of the crack. The parameters used for the model are listed in Table 2 [2]. It can be seen from the table that the existence of cracks weakens the cohesion on both sides of the crack surface.

3. Simulation Results and Analysis

3.1. Strength Characteristics of the Cracked Sandstone Specimen. The full stress-strain curve of the cracked specimens is shown in Figure 8, and the extracted variation of the strength with the precrack angles is shown in Figure 9.

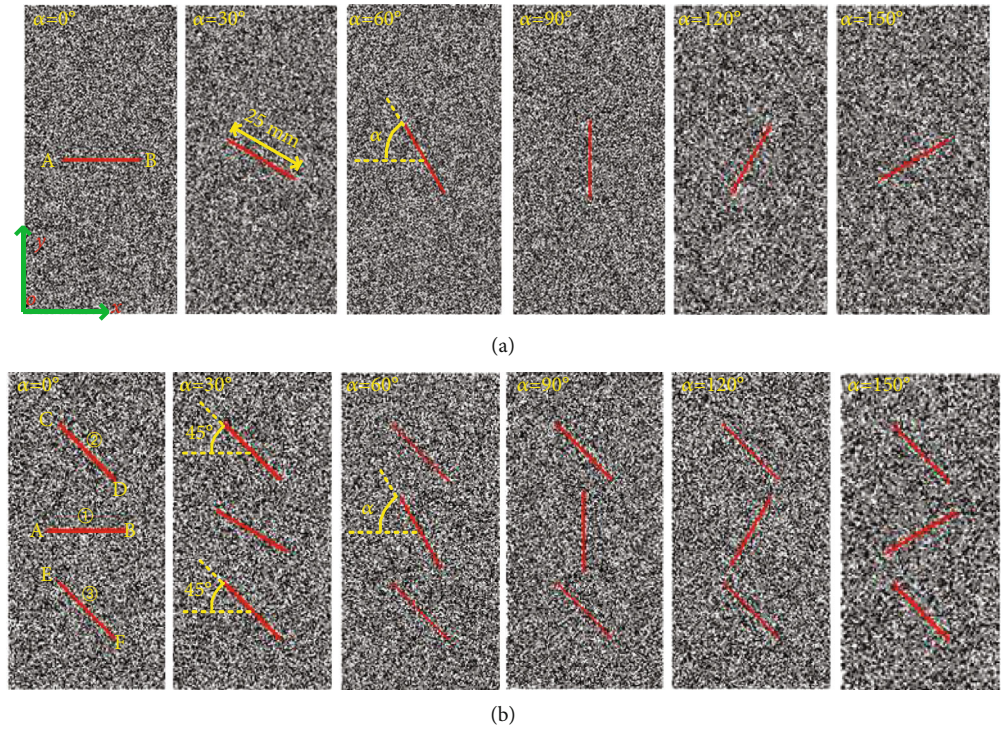

(a)

(b)

Figure 7: Sandstone specimens with a single precrack and three precracks: (a) sandstone specimen with a single precrack; (b) sandstone specimen with three precracks.

Table 2: Mechanical parameters of the smooth joint model [2].

Parameters	Value
Normal stiffness per unit area (GPa)	2
Shear stiffness per unit area (GPa)	2
Friction coefficient	0.35
Tensile strength (Pa)	0
Cohesion (Pa)	0

It can be seen from Figure 8(a) that both the strengths and the elastic moduli of the specimens containing a single crack increase first and then decrease with the increase of the precrack angle. The uniaxial compressive strengths (UCS) of the specimen with the precrack angle of 0°, 30°, 60°, 90°, 120°, and 150° are 21.79 MPa, 26.42 MPa, 33.20 MPa, 49.49 MPa, 40.05 MPa, and 26.47 MPa, respectively, as shown in Figure 9. Theoretically, the specimens with the crack angles of 120° and 60°, as well as the specimens with crack angles of 150° and 30°, are not essentially different, so the elastic moduli of the specimens are almost the same, as shown in Figure 8(a). However, the strengths of the specimens with crack angles of 120° and 60° are quite different, which might be due to the dispersion of the particle and bond distribution inside the specimen [35–37].

The full stress-strain curve and strength value of the specimens with three precracks are shown in Figure 8(b). It can be seen that for the specimen with the precrack angle of 0°, 30°, 60°, 90°, 120°, and 150°, their strengths are 19.6 MPa, 25.4 MPa, 29.3 MPa, 29.1 MPa, 29.10 MPa, and 23.39 MPa, respectively. Compared with the one-crack specimens, the elastic moduli of the specimens change little with the crack angle.

In particular, for the specimens with crack angles of 60°, 90°, and 120°, the difference in their strengths is negligible. Extra uniaxial compression experiments were done on the double-cracked specimens (only including cracks ② and ③, see Figure 9). Results showed that the difference between the strengths of the three precrack specimens and the double-cracked specimen is very small, which indicates that for the specimens with three precracks, the influence of crack ① on the mechanical properties of the specimen can be ignored when the angle of crack ① is in the range of 60° to 120°.

In addition, for both the specimens with a single precrack or three precracks, the smaller the angle between precrack ① and the horizontal direction is, the more fluctuation the full stress-strain curve presents, as shown in Figure 8.

3.2. New Crack Propagation of the Precracked Sandstone Specimen

3.2.1. Initial Crack Propagation. The initial crack propagation of the specimen containing a single precrack is shown in Figure 10. It can be seen that for the specimen with the precrack angle of 0°, new cracks emerge initially in the middle and ends of the precrack, and the development of the new cracks in the middle of the precrack is far quicker than that at the end of the precrack.

For the specimens with the precrack angles of 30° and 60°, new cracks emerge initially at the ends of the precracks,

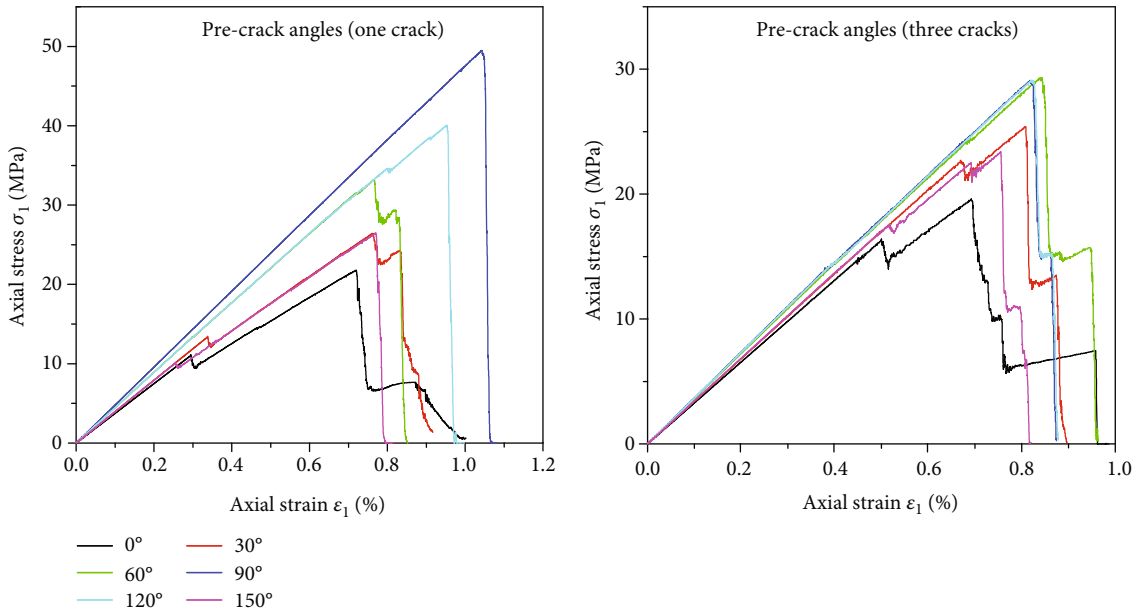

Figure 8: Complete stress-strain curves of the cracked specimens: (a) complete stress-strain curves of the specimens containing a single precrack; (b) complete stress-strain curves of the specimens containing three precracks.

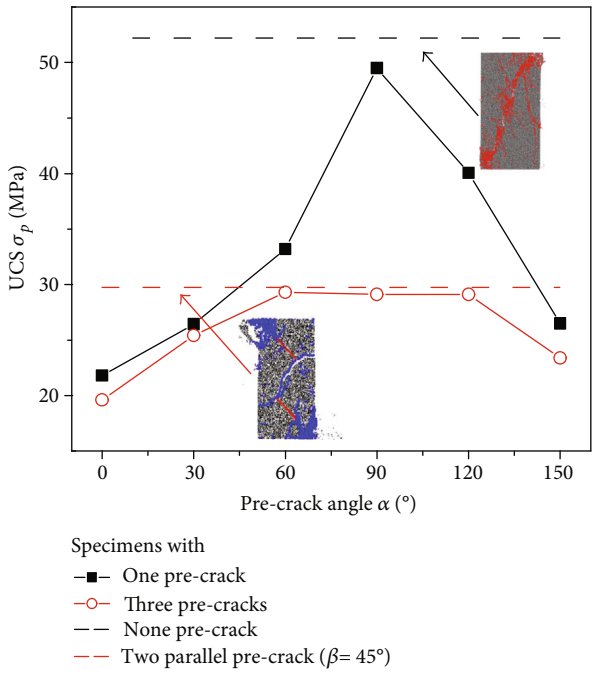

Figure 9: Correspondence between UCS of specimens and precrack angles.

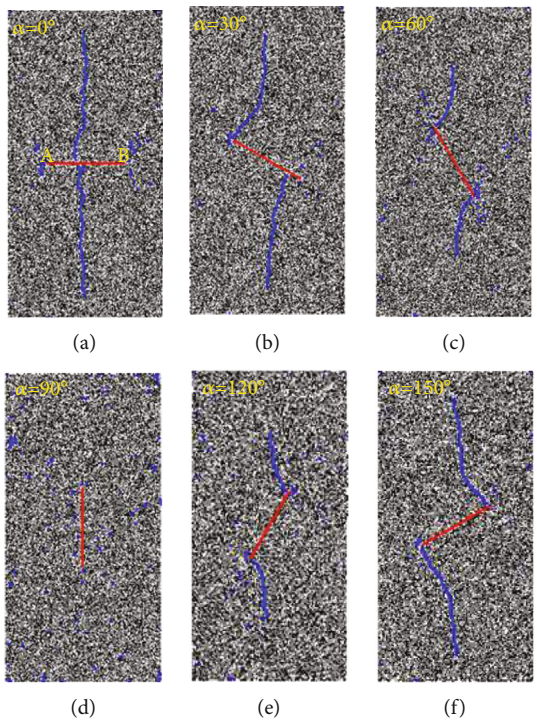

Figure 10: Initial crack propagation of the specimens containing a single precrack.

showing a clear wing expansion. For the specimens with the precrack angle of 90°, new cracks are randomly distributed within the specimen, which indicates that a precrack with the angle of 90° does not cause stress concentration inside the specimen. This is because, under the uniaxial loading condition, the strain and stress distributions of the specimen are uniform on any horizontal section before the specimen is significantly damaged. The crack distribution of the specimens corresponding to Figures 10(e) and 10(f) is symmetrical to the crack distribution of the specimens corresponding to Figures 10(b) and 10(c), respectively, so is the initial crack propagation conditions and thus will not be presented here. Furthermore, it can be clearly seen that as the precrack angle

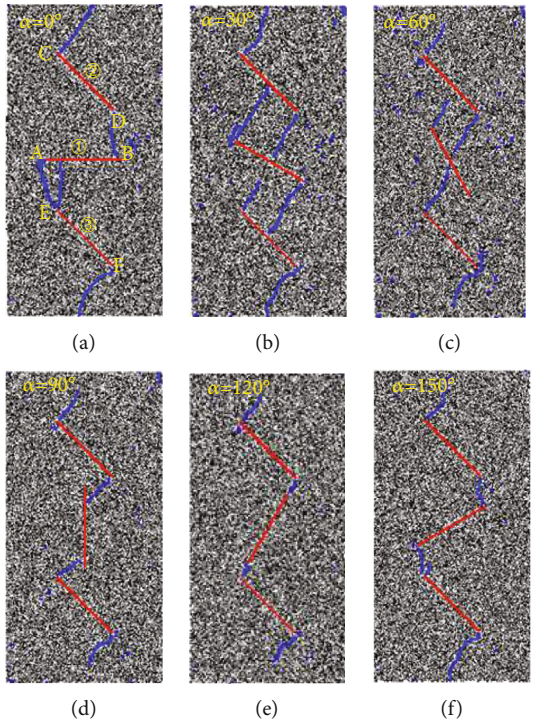

Figure 11: Initial crack propagation of the specimens containing three precracks.

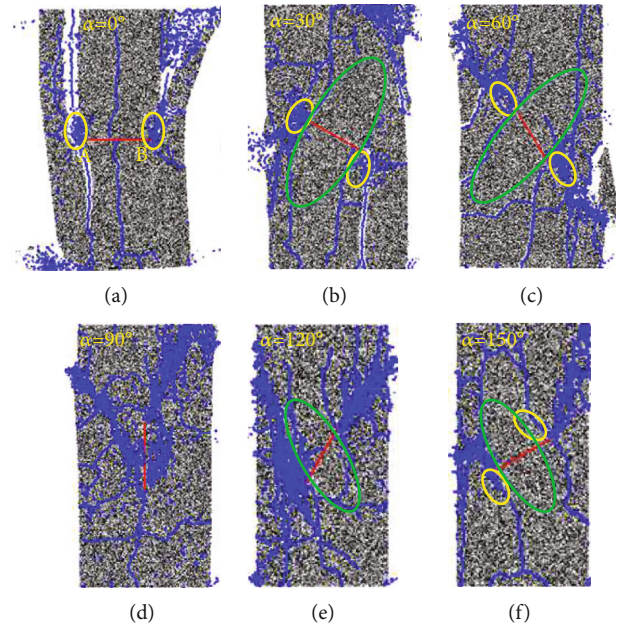

Figure 12: Failure mode of the specimens containing a single precrack.

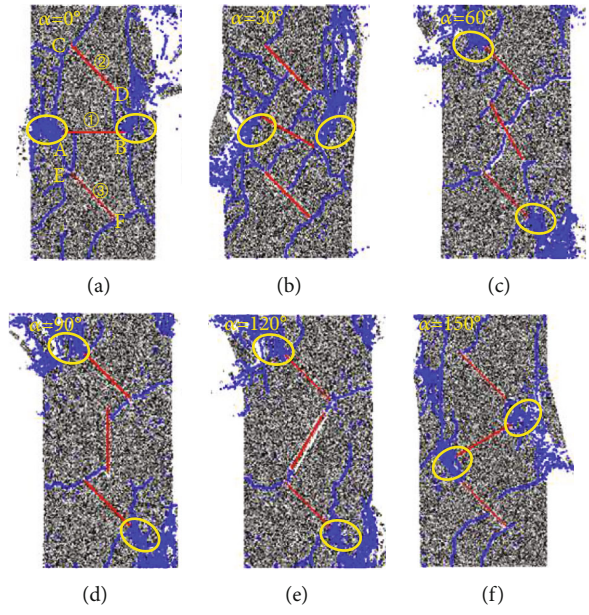

Figure 13: Failure mode of the specimens containing three precracks.

increases from 0° to 90°, the temporal development of the new cracks shows a downward trend, as shown in Figure 10.

The initial crack propagation of the specimens containing three precracks is relatively more complicated, as shown in Figure 11. In general, the new cracks are located at the ends of the precracks, whereas the initial crack distributions at the C-end of crack ② and the F-end of crack ③ remain almost unchanged. The change of the angle of crack ① mainly affects the initial crack propagation of crack ①, the D-end of crack ②, and the E-end of crack ③.

When the angles of crack ① are 0°, 120°, and 150°, the ends of crack ① are closer to the D-end of crack ② and the E-end of crack ③. The two ends of crack ① penetrated with the D-end of crack ② and the E-end of crack ③, as shown in Figures 11(a), 11(e), and 11(f). For the specimen with the crack angle of 30° and 60°, the growth of the initial crack at each crack end is less affected by crack ① as the ends of crack ① are far from the ends of crack ② and crack ③, as shown in Figures 11(b) and 11(c).

When the angle of precrack ① is 90°, the internal stress concentration within the specimen is induced by cracks ② and ③. Compared with the one-crack specimen (see Figure 10(e)), the distribution of new cracks in the specimen is no longer uniform, new cracks of precrack ② of crack ③ penetrate through precrack ①, and there is no new crack propagated from the ends of crack ①.

3.2.2. Failure Modes. The final failure modes of specimens containing a single precrack and three precracks are present in Figures 12 and 13. The final failure modes of the specimens vary substantially with the change of the precrack angle α.

For the single precrack specimens with 0° crack angle α, the failure mode is mostly the vertical splitting failure. Three vertical cracks extended from the two ends, and the middle of the precrack cut the specimen into strips. Moreover, there are many accumulated cracks located at the ends of the precrack, denoted by the yellow ellipses in Figure 12(a). For the specimens with the crack angles of 30° and 60°, their failures are caused by the gradual expansion of the new cracks along

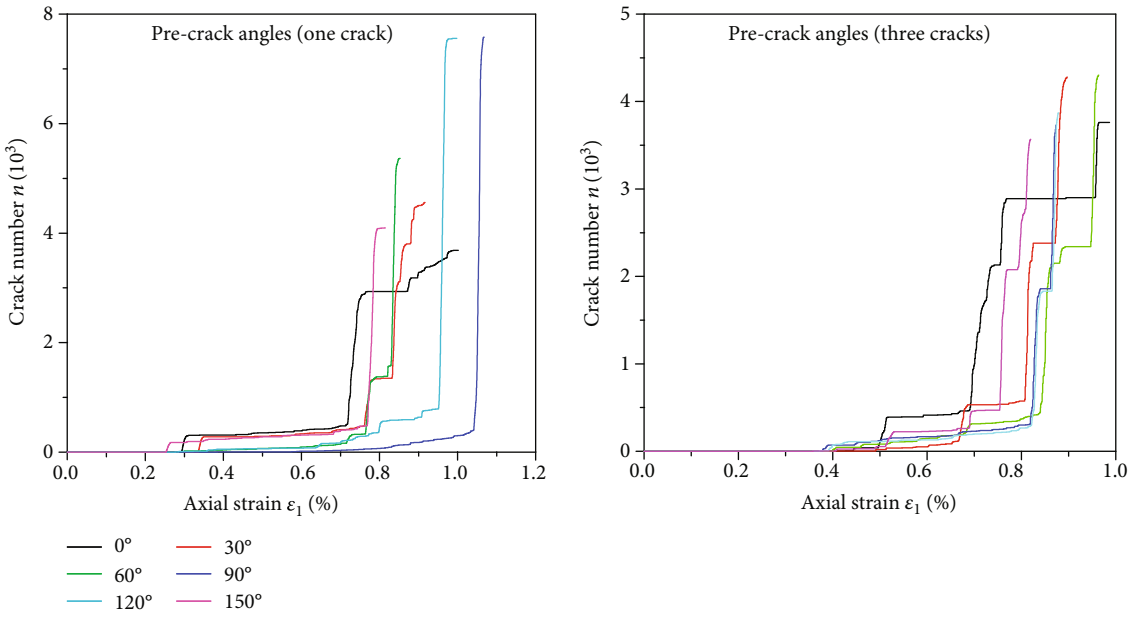

Figure 14: Crack number evolution of the precracked sandstone specimens: (a) crack number evolution of the specimens containing a single precrack; (b) crack number evolution of the specimens containing three precracks.

the ends of the precracks. Quite a few new cracks are closely located at the precrack ends, as highlighted by the yellow ellipses in Figures 12(b) and 12(c). There are few new cracks generated in the vertical direction of the precracks, as shown by the blue ellipses in Figures 12(b) and 12(c). This is agreed with the finding of Shi et al. [2] that nonvertical cracks will form a stress shielding circle with the diameter of its own. For the specimens containing precracks with the angles of 120° and 150°, the failure modes are the same as that of the specimens with the precrack angles of 60° and 30°, respectively, and will not be repeated here. For the specimens with the precrack angle of 90°, the effect of precracks on the failure mode of the specimen is negligible. The failure of the upper right corner of the specimen is very similar to that of the intact specimen (see Figures 6(b) and 12(d)).

For the specimens with three precracks, when the angle of precrack ① is 0°, due to the stress shielding effect of the precracks, there are basically no new cracks that emerged in the area between the adjacent precracks. As shown in Figure 13(a), the ends of the three precracks penetrate through each other, which results in the cutting failure of the specimen [38, 39]. For the specimen with the precrack angle of 30°, the new cracks mainly occurred in the middle of the specimens due to the dense and uniform distribution of the precracks in this area. For the specimen with the precrack angles of 60°, 90°, and 120°, precracks ② and ③ penetrated through precrack ①, and the new cracks mainly concentrated at the C-end of crack ② and the F-end of crack ③. The failure modes of these three specimens are very similar. The failure modes of the specimens with the precrack angles of 150° and 30° are similar, and the concentrated cracks are mainly distributed at the junction of the A-end of crack ① and the D-end of crack ②, as well as the junction of the B-end of crack ① and the E-end of crack ③.

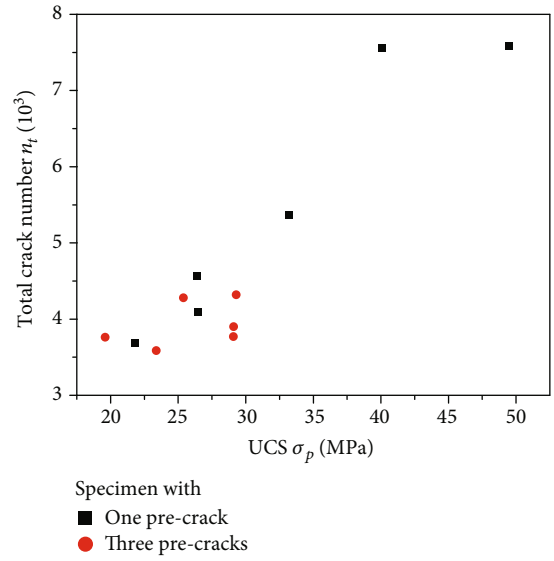

Figure 15: Correspondence between the UCS and the new crack number of the sandstone specimens.

3.3. Crack Number Evolution of the Precracked Sandstone Specimens. New cracks keep emerging in the loading process. The evolution of the number of new cracks (NNC) during loading process is shown in Figure 14. In general, the evolution of NNC exhibits a stair-step tendency, i.e., increases abruptly as the axial strain increases to a

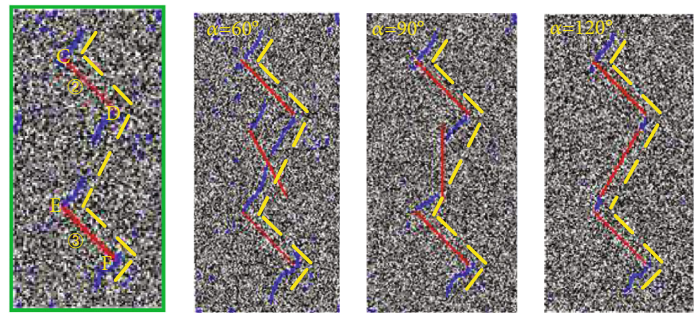

(a) (b) (c) (d)

Figure 16: Comparison of the initial crack propagation of double-crack and triple-crack specimens.

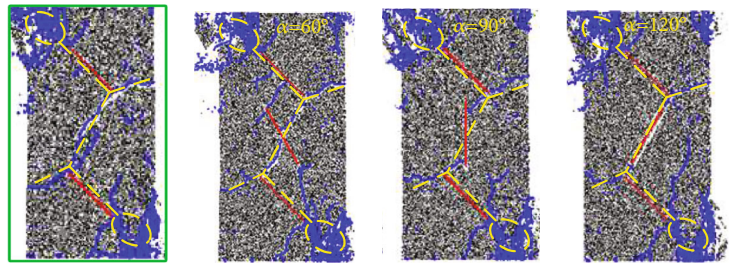

(a) (b) (c) (d)

Figure 17: Comparison of the failure mode of double-crack and triple-crack specimens.

certain value. The NNC evolution of single precrack specimens experiences a one-step (corresponding to precrack angles of 90° and 120°) or two-step (corresponding to precrack angles of 0°, 30°, 60°, and 150°) increase. It can be seen from Figure 14(a) that for the specimen containing a single precrack, the number of new cracks approximately increased in one-step stair shape (corresponding to precrack angles of 60°, 90°, and 120°) or two-step stair shape (corresponding to precrack angles of 0°, 30°, and 150°) with the increase of axial strain. Notably, the maximum abrupt increase in NNC occurs at various axial strains for different precrack angles, i.e., increased axial strain value as the precrack angle increased until 90° and declined thereafter. For the specimens with three precracks (see Figure 14(b)), the evolution of NNC shows a multistep growth, which can be attributed to the fluctuations of the full stress-strain curves of the specimens before and after the peak (see Figure 8(b)).

Interestingly, the NNCs corresponding to the final failure of the specimens with three precracks are around 4000 with extremely small deviation. For the specimens with a single precrack, when the crack angles are 0°, 30°, 60°, and 150°, the final NNCs are closer to 4000 as well. However, when the precrack angles are 90° and 120°, the final NNCs are up to 7500. By extracting the final NNC and UCS of the specimens (see Figures 14 and 9), it was found that the final NNC increased with the UCS, as shown in Figure 15.

4. Discussion

The analysis of Figure 9 in Section 3.1 shows that when the angles α of precrack ① are between 60° to 120°, the effect of precrack ① on the mechanical properties of the specimen can be ignored, which is very interesting and worthy of further study.

The initial crack propagation of the double-crack specimen (see Figure 16(a)) and the triple-crack specimens (see Figures 16(b)–16(d)) are shown in Figure 16. The existence of precrack ① inside the three-crack specimens has little effect on the initial crack growth. The D-end of crack ② and the E-end of crack ③ tend to penetrate in both the double-crack and the triple-crack specimens, and crack ① itself, as the penetration path of crack ② and crack ③, only promoted this process, especially for the specimens whose angles of crack ① are 90° and 120°. Therefore, there is very little difference in the crack distribution (including precracks and newly generated cracks, see the yellow dotted lines in Figure 16) inside the specimens, and the bearing structure of the specimens is very similar, as shown in Figure 16.

Figure 17 shows the failure modes of the double-crack specimen (see Figure 17(a)) and the three-crack specimens (see Figures 17(b)–17(d)). The failure modes of the four specimens in Figure 17 are highly similar. There are many newly generated cracks in the upper left and lower right corners of the specimens (see the yellow ellipses in Figure 17). In addition, the Y-shaped expansion fissures in the upper right and lower left corners are symmetrically distributed with respect to the center point of the specimens (see the yellow dotted lines in Figure 17). In summary, the 4 main rock blocks generated after the failure of the specimen in Figure 17 are almost identical.

For a specific loading condition, the existence of cracks may not necessarily weaken the strength characteristics of

the specimen. From Figures 9, 16, and 17, it can be found that if the precrack does not affect the original crack propagation path (fracture process), it will hardly affect the mechanical properties of the specimen.

5. Conclusions

In this paper, the relationship between the strength characteristics of the specimen and the angle of the precrack, as well as the interaction of cracks under uniaxial compression, was studied. The two sets of sandstone specimens, respectively, containing a single precrack and three precracks were built using the PFC software, which was to study. The main conclusions are as follows:

(1) For the one-crack specimens, the peak strength and elastic modulus continuously increase as the crack angle α is more aligning with the forcing (loading) direction. For the three-crack specimens, a similar pattern was observed for the strength behavior, i.e., with higher strength as α gets closer to the forcing direction. However, such increase stabilized as the angle between α and forcing direction is smaller than 30°. The elastic modulus of the specimens appears to be unaffected by the angles of precrack

(2) For the specimens containing a single precrack, their crack numbers increased approximately in a one-step or two-step stair pattern with increasing axial strain; whereas for the specimens containing three cracks, their crack numbers all showed a multistep stair growth trend with the axial strain

(3) The failure mode of the specimen is closely related to the precrack angle. However, the existence of cracks may not necessarily weaken the strength characteristics of the specimen. If the precrack does not affect the original crack propagation process (fracture process), it will hardly affect the mechanical properties of the specimen

Data Availability

The data used to support the findings of the study are available from the corresponding author upon request.

Conflicts of Interest

All authors declare that they have no conflict of interest or financial conflicts to disclose.

Acknowledgments

The authors gratefully acknowledge the financial support provided by the Independent Research Project of State Key Laboratory of Coal Resources and Safe Mining, CUMT (Grant Number SKLCRSM001).

References

[1] A. Lenton, K. L. McInnes, and J. G. O'Grady, "Marine projections of warming and ocean acidification in the Australasian region," *Australian Meteorological and Oceanographic Journal*, vol. 65, no. 1, pp. S1–S28, 2015.

[2] H. Shi, L. Song, H. Q. Zhang et al., "Numerical study on mechanical and failure properties of sandstone based on the power-law distribution of pre-crack length," *Geomechanics and Engineering*, vol. 19, no. 5, pp. 421–434, 2019.

[3] J. Y. Wu, M. M. Feng, X. B. Mao et al., "Particle size distribution of aggregate effects on mechanical and structural properties of cemented rockfill: experiments and modeling," *Construction and Building Materials*, vol. 193, pp. 295–311, 2018.

[4] M. Asadi and M. H. Bagheripour, "Numerical and intelligent modeling of triaxial strength of anisotropic jointed rock specimens," *Earth Science Informatics*, vol. 7, no. 3, pp. 165–172, 2014.

[5] Q. H. Lei and K. Gao, "A numerical study of stress variability in heterogeneous fractured rocks," *International Journal of Rock Mechanics and Mining Sciences*, vol. 113, pp. 121–133, 2019.

[6] N. E. Odling, "Scaling and connectivity of joint systems in sandstones from western Norway," *Journal of Structural Geology*, vol. 19, no. 10, pp. 1257–1271, 1997.

[7] H. Shi, H. Q. Zhang, L. Song et al., "Failure characteristics of sandstone specimens with randomly distributed pre-cracks under uniaxial compression," *Environmental Earth Sciences*, vol. 79, no. 9, article 193, 2020.

[8] I. J. Basson and G. Viola, "Structural overview of selected group II kimberlite dyke arrays in South Africa: implications for kimberlite emplacement mechanisms," *South African Journal of Geology*, vol. 106, no. 4, pp. 375–394, 2003.

[9] C. Deng, H. X. Hu, T. L. Zhang, and J. L. Chen, "Rock slope stability analysis and charts based on hybrid online sequential extreme learning machine model," *Earth Science Informatics*, vol. 13, no. 3, pp. 729–746, 2020.

[10] Y. H. Huang, S. Q. Yang, and J. Zhao, "Three-dimensional numerical simulation on triaxial failure mechanical behavior of rock-like specimen containing two unparallel fissures," *Rock Mechanics and Rock Engineering*, vol. 49, no. 12, pp. 4711–4729, 2016.

[11] Y. Q. Zhou, Q. Sheng, N. N. Li, X. Fu, Z. Zhang, and L. Gao, "A constitutive model for rock materials subjected to triaxial cyclic compression," *Mechanics of Materials*, vol. 144, article 103341, 2020.

[12] G. W. Chen, L. Song, and R. R. Zhang, "Modeling acoustic attenuation of discrete stochastic fractured media," *Acta Geodaetica et Geophysica*, vol. 53, no. 4, pp. 679–690, 2018.

[13] P. T. Wang, F. H. Ren, and M. F. Cai, "Mechanical analysis and size effect of rough discrete fractures network model under direct shear tests based on particle flow code," *Journal of China Coal Society*, vol. 43, no. 4, pp. 976–983, 2018.

[14] Z. M. Yang, Y. T. Gao, S. C. Wu, Z. Q. Cheng, and A. B. Jin, "Study of the influence of joint parameters on rock mass strength based on equivalent rock mass technology," *Journal of China University of Mining and Technology*, vol. 47, no. 5, pp. 979–986, 2018.

[15] P. A. Cundall and O. D. L. Strack, "A discrete numerical model for granular assemblies," *Géotechnique*, vol. 29, no. 1, pp. 47–65, 1979.

[16] H. Q. Zhang, S. Nunoo, D. D. Tannant, and S. Y. Wang, "Numerical study of the evolution of cohesion and internal friction in rock during the pre-peak deformation process," *Arabian Journal of Geosciences*, vol. 8, no. 6, pp. 3501–3513, 2015.

[17] H. Q. Zhang, D. D. Tannant, H. W. Jing, S. Nunoo, S. J. Niu, and S. Y. Wang, "Evolution of cohesion and friction angle during microfracture accumulation in rock," *Natural Hazards*, vol. 77, no. 1, pp. 497–510, 2015.

[18] R. Vachon and C. F. Hieronymus, "Mechanical energy balance and apparent fracture toughness for dykes in elastoplastic host rock with large-scale yielding," *Geophysical Journal International*, vol. 219, no. 3, pp. 1786–1804, 2019.

[19] F. S. Ren, T. C. Fang, and X. Z. Cheng, "Study on rock damage and failure depth under particle water-jet coupling impact," *International Journal of Impact Engineering*, vol. 139, article 103504, 2020.

[20] S. Q. Yang, Y. Z. Jiang, W. Y. Xu, and X. Q. Chen, "Experimental investigation on strength and failure behavior of pre-cracked marble under conventional triaxial compression," *International Journal of Solids and Structures*, vol. 45, no. 17, pp. 4796–4819, 2008.

[21] H. Yang, H. Lin, Y. Wang, R. Cao, J. Li, and Y. Zhao, "Investigation of the correlation between crack propagation process and the peak strength for the specimen containing a single pre-existing flaw made of rock-like material," *Archives of Civil and Mechanical Engineering*, vol. 21, no. 2, p. 68, 2021.

[22] C. Zhang, Y. Wang, and T. Jiang, "The propagation mechanism of an oblique straight crack in a rock sample and the effect of osmotic pressure under in-plane biaxial compression," *Arabian Journal of Geosciences*, vol. 13, no. 15, p. 736, 2020.

[23] M. Wang, W. Wan, and Y. L. Zhao, "Experimental study on crack propagation and the coalescence of rock-like materials with two preexisting fissures under biaxial compression," *Bulletin of Engineering Geology and the Environment*, vol. 79, no. 6, pp. 3121–3144, 2020.

[24] C. Q. Zhang, Z. J. Liu, Y. B. Pan, Y. Gao, H. Zhou, and G. Cui, "Influence of amygdale on crack evolution and failure behavior of basalt," *Engineering Fracture Mechanics*, vol. 226, article 106843, 2020.

[25] Itasca Consulting Group Inc, *PFC2D (Particle Flow Code in 2 Dimensions): Version 2018, 5.00.35*, Minneapolis, 2018.

[26] L. X. Xiong, Z. Y. Xu, T. B. Li, and Y. Zhang, "Bonded-particle discrete element modeling of mechanical behaviors of interlayered rock mass under loading and unloading conditions," *Geomechanics and Geophysics for Geo-Energy and Geo-Resources*, vol. 5, no. 1, pp. 1–16, 2019.

[27] U. Castro-Filgueira, L. R. Alejano, J. Arzúa, and D. M. Ivars, "Sensitivity analysis of the micro-parameters used in a PFC analysis towards the mechanical properties of rocks," *Procedia Engineering*, vol. 191, pp. 488–495, 2017.

[28] C. B. Jiang, Z. K. Li, W. S. Wang, Z. Wen, M. Duan, and W. Geng, "Experimental investigation of the mechanical characteristics and energy dissipation of gas-containing coal under incremental tiered cyclic loading," *Geomechanics and Geophysics for Geo-Energy and Geo-Resources*, vol. 7, no. 3, 2021.

[29] S. Mukhopadhyay and S. R. Hallett, "A directed continuum damage mechanics method for modelling composite matrix cracks," *Composites Science and Technology*, vol. 176, pp. 1–8, 2019.

[30] J. Y. Wu, M. M. Feng, B. Y. Yu, and G. S. Han, "The length of pre-existing fissures effects on the mechanical properties of cracked red sandstone and strength design in engineering," *Ultrasonics*, vol. 82, no. 1, pp. 188–199, 2018.

[31] Y. Benveniste, "On the Mori-Tanaka's method in cracked bodies," *Mechanics Research Communications*, vol. 13, no. 4, pp. 193–201, 1986.

[32] K. Wang, F. du, X. Zhang, L. Wang, and C. P. Xin, "Mechanical properties and permeability evolution in gas-bearing coal-rock combination body under triaxial conditions," *Environmental Earth Sciences*, vol. 76, no. 24, 2017.

[33] H. Shi, H. Q. Zhang, and L. Song, "Evolution of sandstone shear strength parameters and its mesoscopic mechanism," *Geomechanics and Engineering*, vol. 20, no. 1, pp. 29–41, 2020.

[34] H. Shi, H. Q. Zhang, L. Song, and Y. Wu, "Variation of strata pressure and axial bolt load at a coal mine face under the effect of a fault," *Archives of Mining Sciences*, vol. 64, no. 2, pp. 351–374, 2019.

[35] L. L. Chen, Z. W. Wang, X. Peng, J. Yang, P. Wu, and H. Lian, "Modeling pressurized fracture propagation with the isogeometric BEM," *Geomechanics and Geophysics for Geo-Energy and Geo-Resources*, vol. 7, no. 3, 2021.

[36] Z. Y. Liao, C. A. Tang, W. M. Yang, and J. B. Zhu, "Three-dimensional numerical investigation of rock plate cracking and failure under impact loading," *Geomechanics and Geophysics for Geo-Energy and Geo-Resources*, vol. 7, no. 2, article 33, 2021.

[37] M. Wang, D. J. Zheng, S. J. Niu, and W. Li, "Large deformation of tunnels in longwall coal mines," *Environmental Earth Sciences*, vol. 78, no. 2, 2019.

[38] K. Eshiet and Y. Sheng, "Influence of rock failure behaviour on predictions in sand production problems," *Environmental Earth Sciences*, vol. 70, no. 3, pp. 1339–1365, 2013.

[39] H. Shi, L. Song, W. L. Chen et al., "New non-destructive method for testing the strength of cement mortar material based on vibration frequency of steel bar: theory and experiment," *Construction and Building Materials*, vol. 262, p. 120931, 2020.